Soil Dynamics and Earthquake Engineering 31 (2011) 996–1008

Contents lists available at ScienceDirect

Soil Dynamics and Earthquake Engineering

journal homepage: www.elsevier.com/locate/soildyn

Spectral shape proxies and nonlinear structural response

Edén Bojórquez [a,*], Iunio Iervolino [b]

[a] Facultad de Ingeniería, Universidad Autónoma de Sinaloa, Calzada de las Américas y Boulevard Universitarios s/n, Ciudad Universitaria, Culiacán Rosales, Sinaloa, C.P. 80040, Mexico

[b] Dipartimento di Ingegneria Strutturale, Università degli Studi di Napoli Federico II, Via Claudio 21, 80125 Napoli Italia, Italy

ARTICLE INFO

Article history:
Received 15 September 2009
Received in revised form
22 October 2010
Accepted 8 March 2011
Available online 9 April 2011

ABSTRACT

In this paper, spectral-shape-based intensity measures (*IMs*) are discussed with respect to ordinary, pulse-like and narrow-band records. First, the analyses address the ability of these *IMs* to capture the peak and cumulative damage potentials of ground motions. Second, a new vector-valued ground motion *IM* based on the spectral acceleration at the first mode of the structure, $Sa(T_1)$, and a parameter proxy for the spectral shape, namely N_p, is introduced. The vector $\langle Sa,N_p \rangle$ is compared to other state-of-the-art *IMs* in terms of estimation of the seismic response of nonlinear single degree of freedom systems, reinforced concrete and steel moment resisting frames. Results show that $\langle Sa,N_p \rangle$ may be especially useful to represent the ground motion potential in the case of records with peculiar spectral shape. Further, it is shown that $\langle Sa,N_p \rangle$ has the properties of efficiency, sufficiency and scaling robustness. Finally, a scalar ground motion *IM* based on $Sa(T_1)$ and N_p is also discussed, and the possibility to compute the seismic hazard analysis for it is illustrated.

1. Introduction

Probabilistic seismic demand analysis (PSDA) is part of the procedure to estimate the risk of structures subjected to earthquakes in probabilistic terms. As it is well-known by past studies (e.g. [1–3]) the PSDA can be carried out computing the mean annual frequency (MAF) of exceeding an engineering demand parameter (*EDP*) (e.g. interstory drift ratio, dissipated hysteretic energy or Park and Ang damage index) via an application of the total probability theorem:

$$\lambda_{EDP}(x) = \sum_i v_i \int_{IM}\int_{M}\int_{R} P[EDP > x|IM,M,R] f(IM|M,R)\, f(M,R) dr\, dm\, d(im) \quad (1)$$

where $\lambda_{EDP}(x)$ is the MAF of the *EDP* exceeding the value x, v_i is the rate of earthquakes for a specific seismogenic source i affecting the site of interest, $f(IM|M,R)$ is the conditional probability density function (PDF) of the *IM* given magnitude (M) and the source-to-site distance (R) or a ground motion prediction equation (GMPE), $f(M,R)$ is the joint PDF of M and R; $P[EDP > x|IM,M,R]$ is the probability of *EDP* exceeding x given *IM*, M and R. If $P[EDP > x|IM,M,R] = P[EDP > x|IM]$, then the *IM* is said to be sufficient [1,2] since its ability to predict the structural response is independent of M and R given *IM*. If *IM* is sufficient, Eq. (1) can be expressed as

$$\lambda_{EDP}(x) = \int_{IM} P[EDP > x|IM] |d\lambda_{IM}(im)| \quad (2)$$

where $d\lambda_{IM}(im)$ is the differential of the ground motion hazard curve for the *IM*. Note that *IM* in Eqs. (1) and (2), in general, can not only be a scalar measure, but also a vector-valued. In general, the desirable properties for an *IM* are sufficiency, efficiency and scaling robustness [1–4].

A sufficient *IM* is important because it can be used in the probabilistic structural assessment decoupling the hazard and structural analysis. Efficiency is defined as good explanatory power of the *IM* with respect to some *EDP*; this may help in reducing the number of records used to estimate the structural response with given accuracy. Robustness means that the amplitude (linear) scaling of records does not induce bias in the estimation of the seismic demand.

Because of the interest in relating the structural response to ground motion features, it is a long time since the *IMs* have started being investigated. In 1952, Housner [5] proposed to use the area under the velocity spectrum as an *IM*; some years later Von Thun et al. [6] suggested the area under the acceleration spectrum in the range of period from 0.1 to 0.5 s to assess the seismic response of dams. In the last years, the peak ground acceleration PGA and the spectral acceleration at the first mode period of the structure (hereinafter $Sa(T_1)$ or Sa) became very popular, especially because classical hazard analysis quantifies the seismic threat in terms of probability of exceedance of these quantities.

Recently, other advanced *IMs*, both scalar and vector-valued, which are claimed to overcome some shortcomings of traditional *IMs* (e.g., insufficiency); have been proposed. In particular, the vector $\langle Sa,\varepsilon \rangle$ (where epsilon is the number of standard deviations by which an observed logarithm of spectral acceleration differs

* Corresponding author. Tel./fax: +52 6677134043.
E-mail address: ebojorq@uas.uasnet.mx (E. Bojórquez).

0267-7261/$ - see front matter © 2011 Elsevier Ltd. All rights reserved.
doi:10.1016/j.soildyn.2011.03.006

from the mean logarithmic spectral acceleration of a GMPE), which is also related to the elastic spectral shape, has resulted to be sufficient and efficient in many cases [7]. Nevertheless, Tothong and Luco [8] pointed out its ineffectiveness to predict the response of structures subjected to near-source pulse-like records, and they proposed an advanced scalar *IM* based on the inelastic spectral displacement. It is efficient for ordinary and pulse-like records, at least to predict maximum interstory drifts. However, the evaluation of this parameter requires inelastic response assessment, which is, to date, not practical and for this reason it is not included in the present paper. Another vector-valued *IM* $\langle Sa,R_{T1,T2}\rangle$ (based on the original scalar proposed by Cordova et al. [9], where $R_{T1,T2}$ is the ratio between the spectral acceleration at period T_2 divided by spectral acceleration at period T_1, and T_2 represents a period longer than T_1) has been demonstrated to be appropriate for pulse-like records [10]. In this case, the aim of the spectral acceleration at period T_2 is to provide information about the other portion of the spectrum of the record, according to which the structure may be sensitive to nonlinear behavior. Baker and Cornell [11] also preliminarily explored the geometric mean of spectral acceleration in a range of periods, $Sa_{avg}(T_1\ldots T_N)$, as an *IM*.

All the *IMs* described above represent, or are somehow related to, the spectral shape at one or in a range of periods, which implies the assumption that significant information to predict the nonlinear seismic response of structures is given in the elastic spectrum. Because this depends on the *EDP* chosen, it is investigated further in the paper by means of a vector-valued *IM* based on $Sa(T_1)$ and a parameter named N_p. The potential of the $\langle Sa,N_p\rangle$ vector was assessed in terms of efficiency comparisons with other state-of-the-art *IMs*. Also, the scaling robustness property is discussed in the paper. Note that sufficiency was not investigated since recent studies suggest that $Sa(T_1)$ is sufficient with respect to magnitude and distance [4], which is the first parameter of the vector analyzed here. For the aim of this study, several nonlinear single degree of freedom (SDOF) systems and two reinforced concrete and steel moment resisting frames were considered. The vector $\langle Sa,N_p\rangle$, strongly based on the spectral shape, was found consistent as a predictor of the nonlinear structural response in terms of not only maximum displacement, but also with respect to cumulative demand (which may be important for structures sensitive to cyclic content of ground motion [12–17]) and in the case of records with peculiar spectral features as near-source pulse-like, and narrow-band motions. Moreover, because the use of scalar *IMs* may be easier for practical purposes, a scalar ground motion intensity measure based on $Sa(T_1)$ and N_p is also introduced and its efficiency evaluated. Finally, it is demonstrated how the common probabilistic seismic hazard analysis may be extended to the new scalar measure.

2. Characterizing the spectral shape and N_p

It has been discussed that *IMs* often try to capture the structural response via the spectral shape with different degrees of success. For example, $Sa(T_1)$ is the perfect predictor for the response of elastic SDOF systems, and a good predictor for elastic multi-degree of freedom (MDOF) systems dominated by the first mode of vibration, associated to the T_1 period. Moreover, studies have found the sufficiency of $Sa(T_1)$ with respect to magnitude and distance [2,4]. Nevertheless, $Sa(T_1)$ does not provide information about the spectral shape in other regions of the spectrum, which may be important for the nonlinear behavior (beyond T_1) or for structures dominated by higher modes (before T_1). In the case of nonlinear shaking, the structure may be sensitive, for example, to different spectral values associated with a range of periods for example from the fundamental period to a limit value

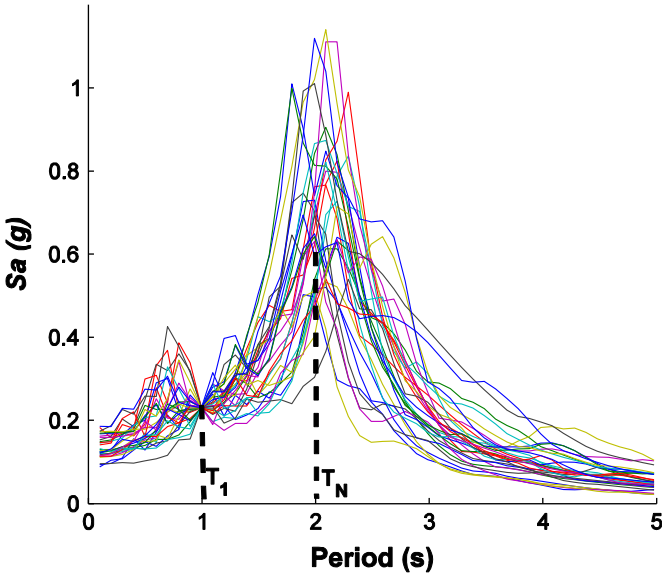

Fig. 1. Response spectra for records scaled to similar $Sa(T_1)$.

of practical interest[1], say T_N. To further illustrate some limitations of $Sa(T_1)$, let us consider a structure with a fundamental period T_1 equal to 1 s subjected to a set of different seismic records scaled to the same $Sa(T_1)$ level. Fig. 1 shows the response spectra of the set of records from the Mexico City case with significant site effects. For this example, the final period is supposed to be T_N equal to 2 s. It can be observed that, although the records have the same $Sa(T_1)$, the spectral ordinates are affected by significant scatter at T_N, which is likely to be reflected in the structural response. This calls for intensity measures providing information about the spectral shape in a whole region of the spectrum as $\langle Sa,R_{T1,T2}\rangle$ and $Sa_{avg}(T_1\ldots T_N)$.

Although parameters such as $Sa_{avg}(T_1\ldots T_N)$ or the area under the spectrum account for the spectral shape, a specific value of $Sa_{avg}(T_1\ldots T_N)$ or area under the spectrum may be associated to different patterns of the spectrum between T_1 and T_N, that is, with different spectral shapes. A useful improvement may be the use of $Sa_{avg}(T_1\ldots T_N)$ but normalizing it by $Sa(T_1)$. To this aim a new parameter named N_p (Eq. (3)) may be introduced:

$$N_p = \frac{Sa_{avg}(T_1\ldots T_N)}{Sa(T_1)} \tag{3}$$

The information given by this equation is that if we have one or n records with a mean N_p value close to 1, we can expect that the average spectrum to be about flat in the period range between T_1 and T_N. For a mean N_p lower than 1 it is expected to have an average spectrum with negative slope. As an example, the mean value of N_p for a group of 191 ordinary records in the period range from $T_1=0.6$ s to $T_N=2T_1$ is 0.39. In Fig. 2a, the average spectrum of this set is illustrated. In the case of N_p values larger than 1, the spectra tend to increase beyond T_1. As it can be appreciated for a set of 31 narrow-band records, where the mean value of $N_p=1.9$ for $T_1=1.2$ s and $T_N=2T_1$, the average spectrum shows an increase in accelerations zone (see Fig. 2b). Finally, for the normalization of $Sa(T_1)$ let N_p be independent of the scaling level of the records based on $Sa(T_1)$, but most importantly it helps to improve the knowledge of the path of the spectrum from period T_1 until T_N, which is related to nonlinear structural response.

[1] It may be also proven that nonlinear structural response is correlated with spectral ordinates at periods lower than the fundamental one.

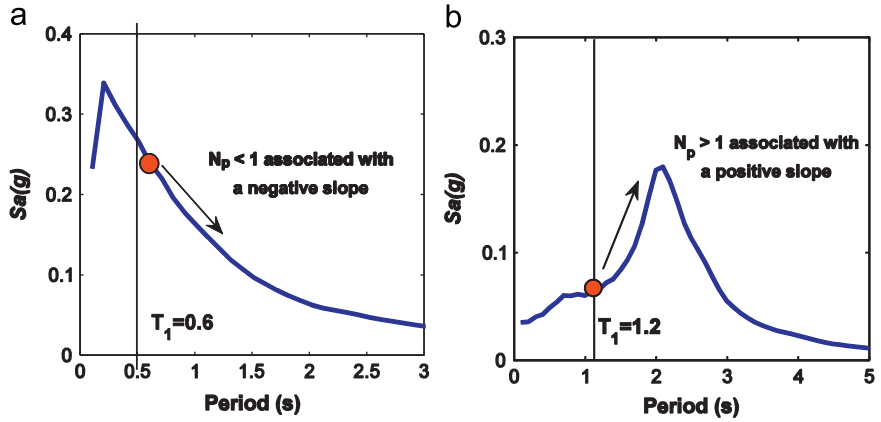

Fig. 2. Mean elastic response spectra for a set of (a) ordinary records with N_p=0.39 and (b) narrow-band records with N_p=1.9.

Table 1
Set of near-source pulse-like records selected from Iervolino and Cornell (2008) [20].

Record no.	Earthquake name	Station name	*Mw*	T_p	PGA (g)
1	San Fernando	Fairmont Dam	6.61	1.05	0.114
2	San Fernando	Lake Hughes #1	6.61	1.15	0.144
3	San Fernando	Lake Hughes #4	6.61	1.05	0.154
4	Point Mugu	Port Hueneme	5.65	1.34	0.100
5	Hollister-03	San Juan Bautista, 24 Polk St	5.14	0.80	0.120
6	Oroville-02	Oroville Airport	4.79	1.25	0.019
7	Oroville-03	Up & Down Cafe (OR1)	4.70	0.92	0.101
8	Friuli, Italy-02	Buia	5.91	0.89	0.109
9	Coyote Lake	Gilroy Array #6	5.74	1.21	0.452
10	Coyote Lake	SJB Overpass, Bent 3 g.l.	5.74	0.83	0.097
11	Coyote Lake	SJB Overpass, Bent 5 g.l.	5.74	0.81	0.074
12	Imperial Valley-07	Bonds Corner	5.01	0.99	0.098
13	Imperial Valley-07	Brawley Airport	5.01	0.82	0.0357
14	Imperial Valley-07	El Centro Array #6	5.01	0.77	0.366
15	Imperial Valley-07	El Centro Array #7	5.01	0.76	0.187
16	Livermore-02	San Ramon—Eastman Kodak	5.42	1.09	0.171
17	Anza (Horse Canyon)-01	Anza Fire Station	5.19	0.78	0.067
18	Mammoth Lakes-06	Long Valley Dam (Upr L Abut)	5.94	1.05	0.400
19	Mammoth Lakes-07	Green Church	4.73	0.81	0.133
20	Mammoth Lakes-08	Fish & Game (FIS)	4.80	0.92	0.128
21	Taiwan SMART1(5)	SMART1 O07	5.90	1.34	0.085
22	Mammoth Lakes-10	Convict Creek	5.34	1.44	0.135
23	Coalinga-02	Harris Ranch—Hdqtrs (temp)	5.09	0.77	0.060
24	Coalinga-05	Oil Fields Fire Station—FF	5.77	1.04	0.227
25	Coalinga-05	Oil Fields Fire Station—Pad	5.77	1.18	0.233
26	Coalinga-05	Transmitter Hill	5.77	0.92	0.859
27	Morgan Hill	Coyote Lake Dam (SW Abut)	6.19	0.95	0.814
28	Drama, Greece	Drama (bsmt)	5.20	1.12	0.056
29	N. Palm Springs	North Palm Springs	6.06	1.38	0.670
30	San Salvador	Geotech Investigation Center	5.80	0.86	0.846
31	Whittier Narrows-01	Compton—Castlegate St.	5.99	0.78	0.342
32	Whittier Narrows-01	Downey—Co Maint Bldg.	5.99	0.79	0.234
33	Whittier Narrows-01	LA—W 70th St.	5.99	0.90	0.193
34	Whittier Narrows-01	LB—Orange Ave.	5.99	0.95	0.255
35	Whittier Narrows-01	LB—Rancho Los Cerritos	5.99	0.92	0.176
36	Whittier Narrows-01	Lakewood—Del Amo Blvd.	5.99	0.95	0.285
37	Whittier Narrows-01	Norwalk—Imp Hwy, S Grnd.	5.99	0.83	0.236
38	Whittier Narrows-01	Santa Fe Springs—E. Joslin	5.99	0.76	0.399
39	Whittier Narrows-02	Inglewood—Union Oil	5.99	0.76	0.153
40	Northridge-01	Pacoima Dam (upper left)	6.69	0.90	1.38
41	Northridge-01	Rinaldi Receiving Sta.	6.69	1.23	0.87
42	Sierra Madre	LA—City Terrace	5.61	1.18	0.01
43	Sierra Madre	San Marino—SW Academy	5.61	1.04	0.146
44	Northridge-06	Sylmar—Converter Sta.	5.28	0.84	0.225
45	Northwest China-02	Jiashi	5.93	0.78	0.163
46	Northwest China-03	Jiashi	6.10	1.34	0.266
47	San Juan Bautista	Hollister—SAGO Vault	5.17	0.95	0.088
48	Big Bear-02	Seven Oaks Dam Right Abt.	4.53	1.14	0.007

Herein, a vector-valued *IM* based on $Sa(T_1)$ and N_p is explored. The vector $\langle Sa,N_p \rangle$ has the following characteristics:

1. the vector is consistent, which means that scaling records for similar $Sa(T_1)$ values and the seismic response will depend on the value of N_p;
2. the vector is relatively efficient independently of the ground motion characteristics (e.g., ordinary, near-source pulse-like and narrow-band motions), or the *EDP* considered (maximum or parameters related with cyclic demand on structures), as it will be illustrated in the following sections;
3. finally, there is a clear relationship between the values of N_p and the spectral shape in a range of periods.

For the case of the vector $\langle Sa,N_p \rangle$, the MAF of *EDP* exceeding a value of x can be computed by using the next equation:

$$\lambda_{EDP}(x) = \int_{Sa}\int_{N_p} P[EDP > x|Sa(T_1),N_p]f(N_p|Sa(T_1))dn_p|d\lambda_{Sa}(sa)| \quad (4)$$

where $f(N_p|Sa(T_1))$ is the conditional distribution function of N_p given $Sa(T_1)$. $P[EDP > x|Sa(T_1),N_p]$ is the probability of *EDP* exceeding x given $Sa(T_1)$ and N_p from structural analysis. Finally, $d\lambda_{Sa}(sa)$ is the differential of ground motion hazard curve in terms of $Sa(T_1)$.

3. Ground motion records and structural models

To explore the intensity measure introduced, three sets of seismic records were considered to represent ordinary, near-source pulse-like and narrow-band motions as these categories may represent systematically different spectral shapes. The set of ordinary records used here was collected by Tothong [18]. The ground motion records were originally obtained from the NGA database. The closest distance to fault rupture is 15–95 km, and the moment magnitude ranges from 5.65 to 7.90.

The pulse-like records consist of a set of 48 motions with a pulse period close to 1 s (mean $T_p \approx 1.0$ s) according to Baker [19]. To warrant that they correspond to near-source pulse-like records, they were rotated in the fault-normal direction. The earthquake magnitude range is 5.6–7.6, and the closest distance to fault rupture is less than 22 km. The pulse-like set is a subset of that in [20]. The principal characteristics of the set of pulse-like records are described in Table 1. Both ordinary and pulse-like records correspond to firm soil or rock.

Narrow-band motions have the special characteristic of affecting considerably structures within a specific range of vibration periods, especially those that soften into or near the narrow-band periods. In fact, these records demand large energy dissipation capacity in structures if compared to broad-band motions [14]. A special case where narrow-band motions are generated corresponds to Mexico City. In this study, a set of 31 ground motion records obtained from the soft-soil of the Valley of Mexico was used. The magnitude range is 6.9–8.1. The records, previously used in [15], correspond to the far field and they were selected for a soil period close to 2 s where the most of the damages in buildings caused by the 1985 Mexican Earthquake were observed.

Regarding structural models, nonlinear SDOFs, reinforced concrete and steel moment resisting frames are analyzed. The SDOFs correspond to systems with different vibration periods, bilinear hysteretic behavior, 5% of post-yielding stiffness and 5% damping ratio. A reinforced concrete (*R*/*C*) frame with 3 bays and 5 stories and a seismic coefficient (ratio between the base shear at yielding divided by the seismic weight) equal to 0.3 are also studied. The height of the first story is 4, and 3 m for the rest of the stories. The width of the bays is 5 m. The trilinear SINA [21] degrading hysteretic behavior model was used in the *R*/*C* elements of the frame with first mode vibration period equal to $T_1 = 0.66$ s and a critical damping of 5%. The steel frame designed with the requirements of the Mexican City Building Code was used in a previous study [22]. The first mode vibration period is 1.20 s, and it has 3 bays and 8 stories. The height of all the stories is 3.5 m and the width of the bays is 8 m. A bilinear hysteretic behavior with 3% of post-yielding stiffness and 3% of critical damping is used. In the case of the MDOF structures, P–δ effects were considered. Table 2 summarizes the principal properties

Table 2
Summary of the structural models.

Structural model	Period, T_1 (s)	Hysteretic behavior model	Damping (% of critical)
SDOF	Different values	Bilinear	5
5 stories *R*/*C* frame	0.66	Trilinear SINA	5
8 stories steel frame	1.20	Bilinear	3

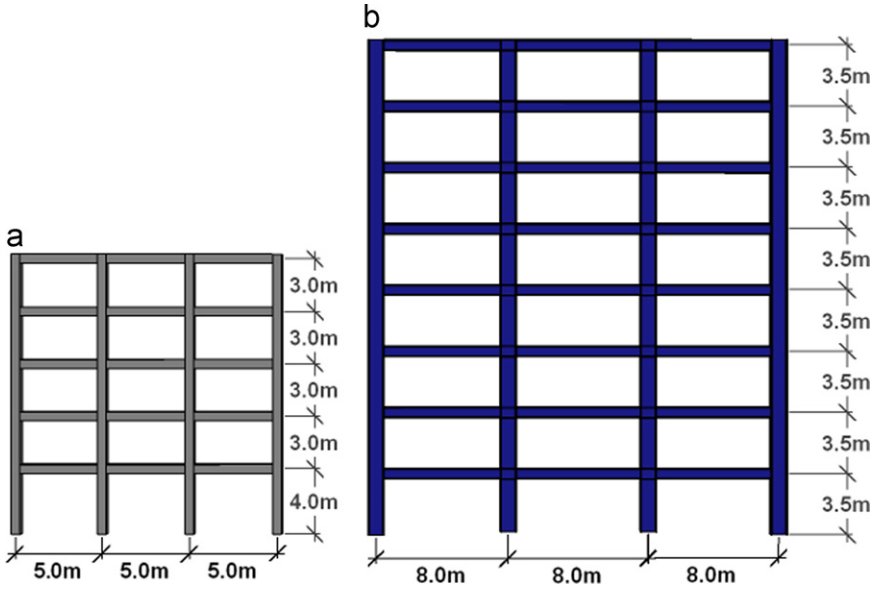

Fig. 3. (a) *R*/*C* ($T_1 = 0.66$ s) and (b) steel frame ($T_1 = 1.20$ s) considered for the dynamic analysis.

of each model, and Fig. 3 illustrates the geometrical characteristics of the *R/C* and steel frames considered.

4. Engineering demand parameters

The *EDPs* considered here are the ductility displacement demand μ_D (evaluated as the ratio between the maximum displacement at the roof and the yielding displacement D_y) and the maximum interstory drift ratio. These parameters were chosen due to their relevance for design purposes; nevertheless, parameters related to the ground motion duration are also considered. The third *EDP* is the normalized dissipated hysteretic energy (N_{EH}) by yielding displacement and strength (F_y); see Eq. (5). N_{EH} was selected here as an *EDP* due to the direct relationship between normalized dissipated hysteretic energy and the cumulative demand [23]. It is important to say that for MDOF systems, F_y and D_y were obtained from a push-over analysis, and E_H corresponds to the total plastic energy dissipated by the structure (the plastic energy dissipated by all the elements).

$$N_{EH} = \frac{E_H}{F_y D_y} \tag{5}$$

The response in terms of the Park and Ang damage index (I_{DPA}) [24] is also analyzed. The expression of I_{DPA} is illustrated in Eq. (6); in this equation μ and μ_D are the monotonic ductility capacity and maximum ductility demand of the system, respectively, and β is a parameter that represents the contribution of dissipated hysteretic energy to the damage, $\beta=0.15$ was considered [25].

$$I_{DPA} = \frac{\mu_D}{\mu} + \beta \frac{E_H}{F_y\, D_y\, \mu} \tag{6}$$

5. Selection of T_2 and T_N from regression analysis

The optimal values of T_2 and T_N, for $R_{T1,T2}$ and N_p, respectively, are analyzed as in [26]. First, dynamic analyses are performed using records scaled to a target $Sa(T_1)$ level. The fractional reduction in the standard deviation of the logarithms of *EDP*, with respect to the case of $Sa(T_1)$ alone, can be computed for the different values of maximum period selected. The optimal T_2 and T_N will be those causing the largest fractional reduction. Note that the standard deviation is computed by means of linear regression of the logarithms of *EDP*.

Cordova et al. [9,27] identify as adequate a T_2 value equal to twice the first mode period, and [28] confirm this for nonlinear SDOF systems and considering different *EDPs*. It may be argued that T_2 generally depends on the nonlinearity level developed in the structure, but $T_2=2T_1$ seems to be appropriate.

Herein, the fractional reduction in dispersion is evaluated for the *R/C* frame subjected to a subset of 40 records chosen randomly from the set of 194 ordinary ground motions. The results for the maximum interstory drift are plotted in Fig. 4a scaling the records to $Sa(T_1)=1$ g. Note that this target spectral acceleration was considered only for illustrative purposes; however, different targets $Sa(T_1)$ are later discussed in this study, the same observation is valid for other cases. The abscissa corresponds to the values of T_2 associated to the vector $\langle Sa,R_{T1,T2}\rangle$ and T_N for the vector $\langle Sa,N_p\rangle$.

First, it can be observed that the optimum value $T_2=2T_1$ may still be considered adequate. For T_N associated to the vector $\langle Sa,N_p\rangle$, the results for the MDOF concrete frame suggest that T_N around 2 or 2.5 times T_1 is an acceptable value. Furthermore, the plots illustrate that using the vector $\langle Sa,N_p\rangle$ the fractional reduction in dispersion increases if compared to $\langle Sa,R_{T1,T2}\rangle$.

Fig. 4b shows the fractional reduction in dispersion for maximum interstory drift and the *R/C* frame subjected to the set of pulse-like records scaling to a target $Sa(T_1)=1$ g. As in the case of maximum interstory drift for ordinary records, the value $T_2=2T_1$ is confirmed in these results. Also, the value of T_N around 2 or 2.5 times T_1 seems adequate.

It is interesting to note how the dispersion can be reduced, with the vectors $\langle Sa,R_{T1,T2}\rangle$ [10] and $\langle Sa,N_p\rangle$, to about 70% with respect to the dispersion obtained through the simple scaling criteria based on the use of $Sa(T_1)$ alone. Furthermore, the efficiency of both parameters $R_{T1,T2}$ and N_p is similar; nevertheless,

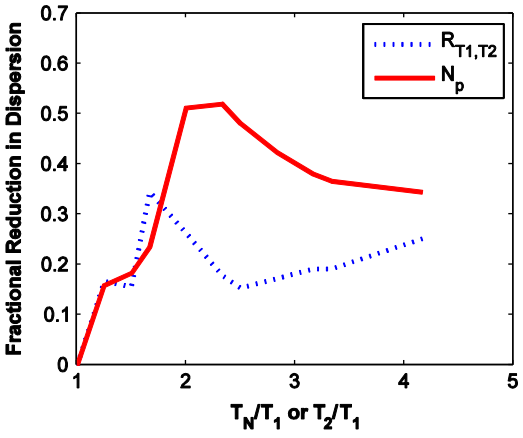

Fig. 5. Fractional reduction in dispersion of maximum interstory drift versus T_N/T_1 and T_2/T_1 for $Sa(T_1)=0.8$ g (8 story steel frame subjected to narrow-band motions).

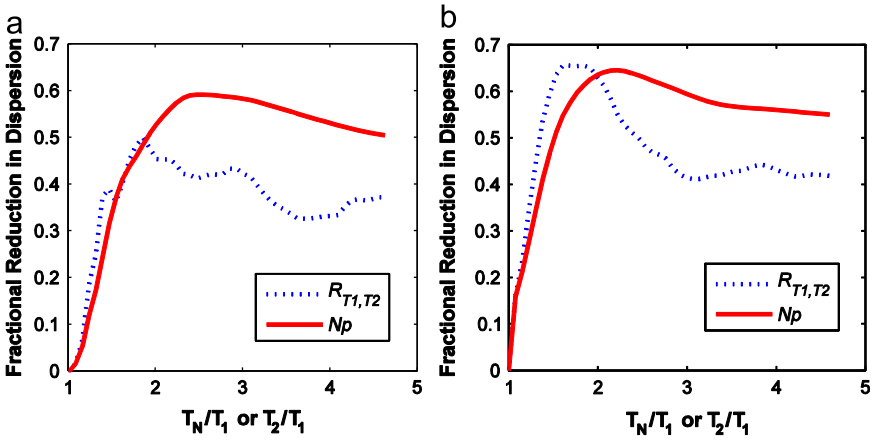

Fig. 4. Fractional reduction in dispersion of maximum interstory drift versus T_N/T_1 and T_2/T_1 for $Sa(T_1)=1$ g; *R/C* frame subjected to (a) ordinary records and (b) pulse-like records.

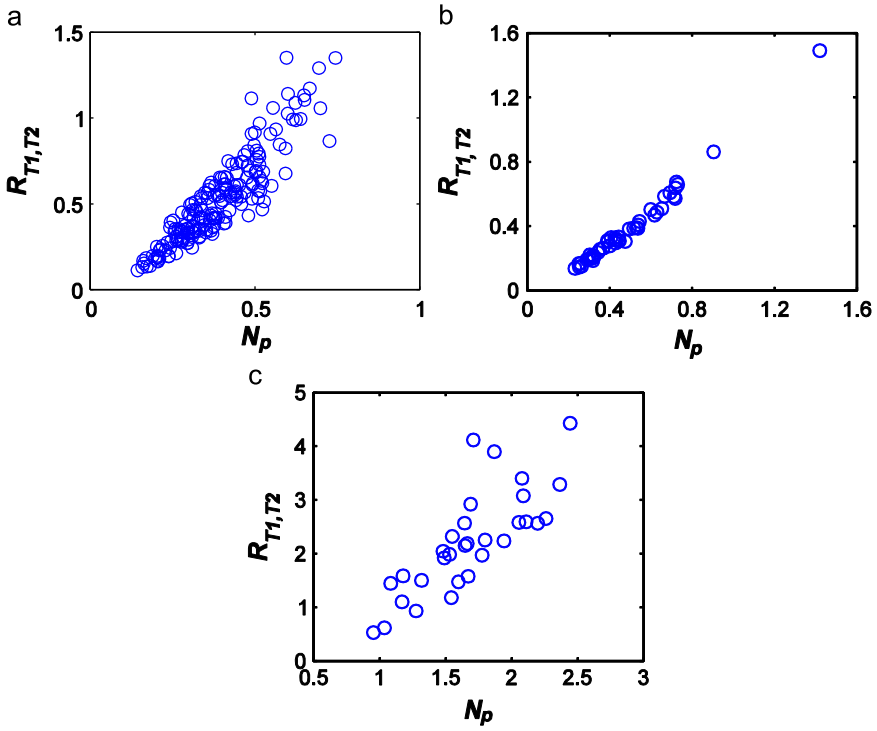

Fig. 6. Relation between N_p versus $R_{T1,T2}$ for (a) ordinary, (b) pulse-like and (c) narrow-band records.

the use of N_p is less sensible to the final period selected if compared to $R_{T1,T2}$, unless T_N values near to T_1 are selected.

The steel structure was subjected to the set of narrow-band motions recorded on Mexico City. The results for maximum interstory drift are plotted in Fig. 5 for $Sa(T_1)=0.8$ g. The fractional reduction in dispersion is quite large when using N_p instead of $R_{T1,T2}$. Also these results suggest that the values of $T_2=2T_1$ and $T_N \geq 2\ T_1$ are reasonable. In general, the same conclusions hold for all the *EDPs* and ground motion characteristics studied, which were not included for the sake of brevity.

Figs. 4 and 5 illustrate the benefits of vector-valued intensity measures, in particular the fractional reduction in dispersion is larger with N_p for ordinary and narrow-band records. To understand these differences, Fig. 6 shows the relationship between the parameters N_p and $R_{T1,T2}$. For the case of pulse-like records both parameters are very well correlated; it explains why the fractional reduction in dispersion is quite similar for both parameters and this set of records. In the case of ordinary and narrow-band records, there is a difference between the values of N_p and $R_{T1,T2}$, particularly for narrow-band records, which is reflected in the results of the fractional reduction in dispersion and also in the efficiency to estimate the structural response as it will be discussed below.

6. Evaluating the efficiency of $\langle Sa,N_p \rangle$ versus $\langle Sa,R_{T1,T2} \rangle$

An efficient *IM* can help to considerably reduce the number of analyses required to estimate the response of structures subjected to earthquakes with a given accuracy. In fact, given that the dispersion of an *EDP* given some intensity measure, the standard error associated to a sample of size n can be expressed as [29]

$$SE = \frac{\sigma_{\ln EDP|IM}}{\sqrt{n}} \tag{7}$$

Eq. (7) means that, reducing the dispersion by 70% as in the case of pulse-like records (Fig. 4), the number of records employed in the vector case is reduced more than 10 times with respect to the use of $Sa(T_1)$ alone ($n_{vector}=0.09n_{scalar}$).

In this section, the efficiency of the vectors $\langle Sa,R_{T1,T2} \rangle$ and $\langle Sa,N_p \rangle$, as predictors of the *EDPs* selected to represent maximum and cumulative demands, is compared. The steel and concrete MDOF structures considered were subjected to the sets of records that represent different characteristics of ground motion. The T_2 and T_N values correspond to the optimal values obtained in the analyses above.

The efficiency is expressed by the maximum fractional reduction in the standard deviation of the logarithms of *EDP*, and then it is compared for all the groups of records considered herein. Fig. 7a compares, for the *R*/*C* frame, the maximum fractional reduction in dispersion of maximum interstory drift at different intensity levels expressed as fractions of g. As it was expected, the vectors reduce considerably the standard deviation compared with the scalar $Sa(T_1)$ for all the ground motion intensity levels considered.

In general the vector $\langle Sa,N_p \rangle$ seems to be more promising when compared to $\langle Sa,R_{T1,T2} \rangle$, especially for the steel structure subjected to narrow-band motions, where the maximum fractional reduction in dispersion for N_p is, in some cases, more than 0.5 when the intensity level increases and for $R_{T1,T2}$ is around 0.3 (see Fig. 7b). In the case of pulse-like records, the results are quite similar for both vectors compared.

6.1. Ordinary records

A SDOF with $T_1=0.6$ s and seismic coefficient at yielding equal to 0.182 was analyzed. The seismic coefficient was selected to achieve a nonlinear behavior with a median ductility of 6 when the structure is subjected to the set of ordinary records scaled to $Sa(T_1)=1$ g.

The *R*/*C* frame was also subjected to the set of ordinary records. While the SDOF was analyzed considering all the ground motions in the set, the *R*/*C* was subjected to a subset of 40 records. For the first case (SDOF), the set of 194 ordinary records was

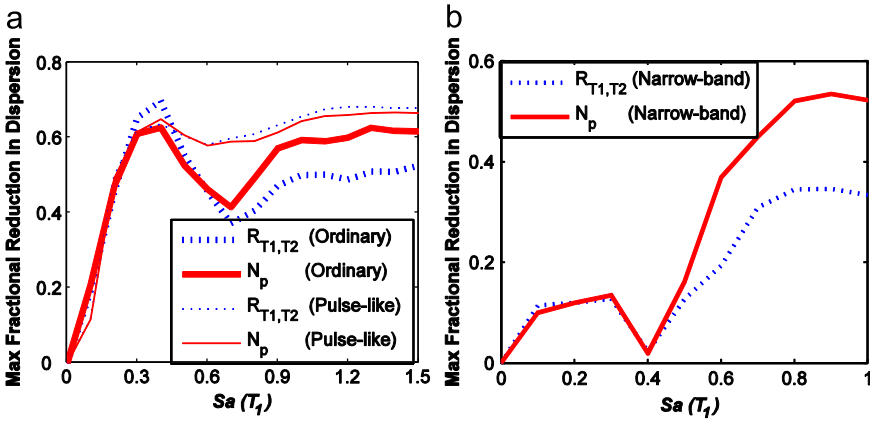

Fig. 7. Maximum fractional reduction in dispersion of maximum interstory drift at different intensity levels for (a) *R*/*C* frame subjected to ordinary and pulse-like records and (b) steel frame under narrow-band records.

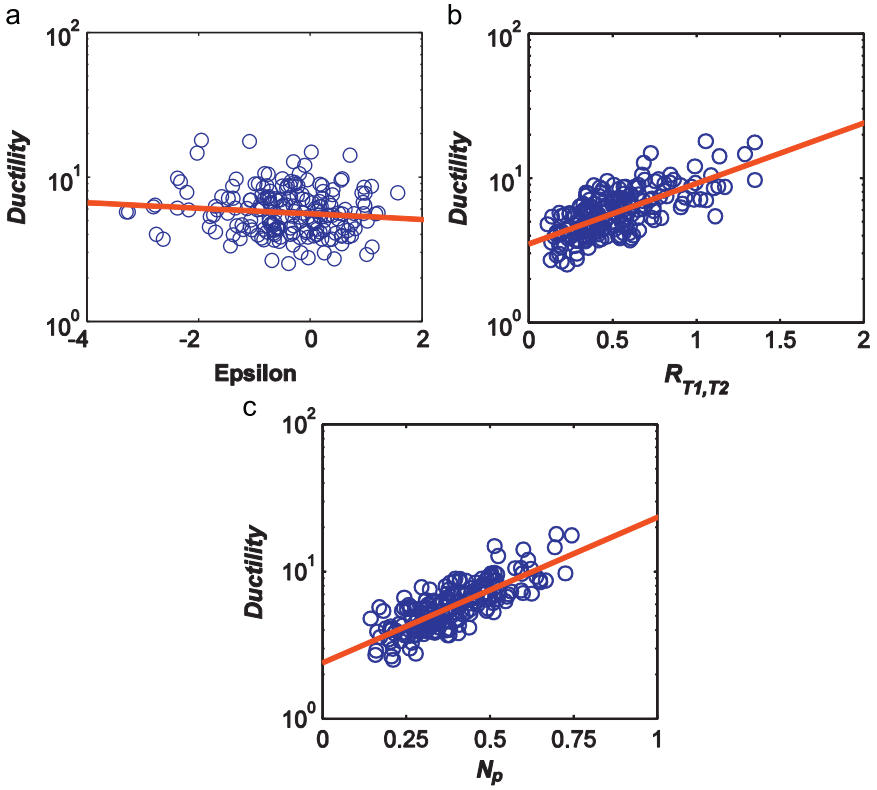

Fig. 8. Ductility prediction for a SDOF with $T=0.6$ s ($Sa=1$ g) for: (a) epsilon, (b) $R_{T1,T2}$ and (c) N_p.

scaled to $Sa(T_1)$ equal to 0.7 g (where the median I_{DPA} is equal to 1) and then the relations between the second parameter of the vector and the different *EDPs* are given. Fig. 8 and 9 show the relationship between epsilon $R_{T1,T2}$ and N_p with the ductility and I_{DPA}. A good correlation exists with all the parameters, especially for N_p, where the efficiency is moderately larger if compared to $R_{T1,T2}$, and it is more related compared with epsilon. However, it is necessary to demonstrate that all the conclusions are valid for a wider range of intensity levels also. Fig. 10a shows the standard deviation of the natural logarithm of I_{DPA} for $Sa(T_1)$ and the vectors $\langle Sa,\varepsilon\rangle$, $\langle Sa,R_{T1,T2}\rangle$ and $\langle Sa,N_p\rangle$. The vector $\langle Sa,N_p\rangle$ results in less dispersion independent of the scaling level of the records. Note also that, while $Sa(T_1)$ and the vectors $\langle Sa,\varepsilon\rangle$ and $\langle Sa,R_{T1,T2}\rangle$ tend to increase the dispersion, the vector $\langle Sa,N_p\rangle$ keeps the standard deviation constant for larger values of intensity level. The same conclusion is valid in the case of ductility demand, which is illustrated in Fig. 10b for different intensity levels. It is observed in Figs. 8–10 that the vectors $\langle Sa,R_{T1,T2}\rangle$ and $\langle Sa,N_p\rangle$ are most correlated to the nonlinear structural response, and for this reason in this paper the efficiency comparison is focused in these two ground motion intensity measures.

The maximum interstory drift for the *R*/*C* frame subjected to the subset of 40 ordinary records scaled at different $Sa(T_1)$ values confirms the conclusion derived for the SDOF system (see Fig. 11). The vectors based on $\langle Sa,N_p\rangle$ and $\langle Sa,R_{T1,T2}\rangle$ allow to estimate with better accuracy the maximum interstory drift for the MDOF concrete frame if compared to $Sa(T_1)$, but the vector based on N_p reduces the heterogeneity associated to the structural response at larger intensity levels. For example, the dispersion in the case of N_p for $Sa(T_1)=1$ g is 0.157, and for $R_{T1,T2}$ it is equal to 0.193 in logarithmic terms. It is illustrated in Fig. 12, where also the correlation between N_p and the maximum interstory drift may be

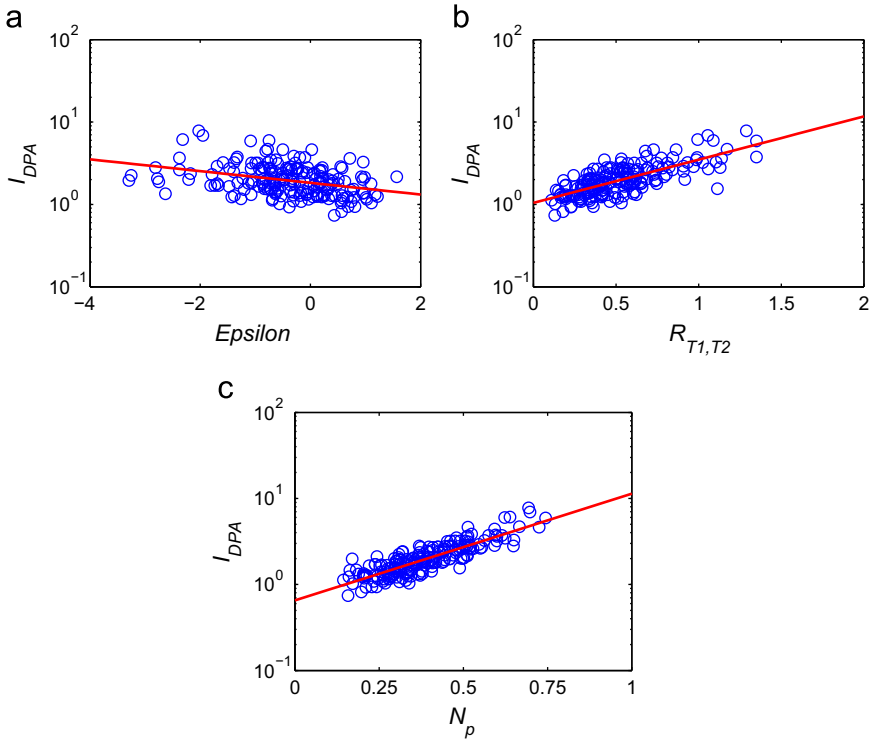

Fig. 9. I_{DPA} prediction for a SDOF with $T=0.6$ s ($Sa=0.7$ g) for (a) epsilon, (b) $R_{T1,T2}$ and (c) N_p.

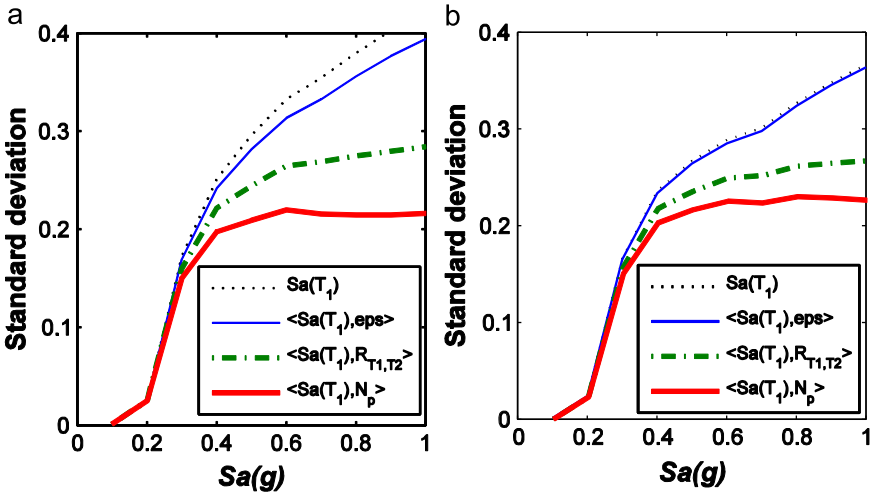

Fig. 10. Standard deviation of the natural logarithm of structural response given $S_a(T_1)$ and the vectors $\langle Sa,\varepsilon\rangle$, $\langle Sa,R_{T1,T2}\rangle$ and $\langle Sa,N_p\rangle$ at different intensity levels for (a) I_{DPA} and (b) ductility demand (SDOF, $T=0.6$ s).

appreciated. All these imply that the number of records used for dynamic analysis in the case of N_p is reduced to nearly 70% if compared to the number of records used for $R_{T1,T2}$; $n\langle_{Sa,Np}\rangle=0.66\ n\langle_{Sa,RT1,T2}\rangle$. In the case of the scalar $Sa(T_1)$ the standard deviation of the natural logarithm is equal to 0.387. That is, the number of records for nonlinear dynamic analysis is reduced more than 80% using the vector $\langle Sa,N_p\rangle$ compared with the scalar Sa.

6.2. Near-source pulse-like records

It was observed that near-source pulse-like records may be threatening for structures where the ratio of the fundamental period and that of the pulse of the record is about one-half ($T_1/T_p=0.5$) [30–32]. Then, it is expected that the R/C frame subjected to the set of 48 motions has an increment of inelastic demand because the structural vibration period is equal to ($T_1=0.66$ s) while the pulse period average is 1 s (mean $T_p\approx 1.0$ s). For this reason, the R/C frame was analyzed when subjected to the pulse-like records. Fig. 13 shows the relationships between the intensity measure parameters studied and the maximum interstory drift up to $Sa(T_1)=1$ g. Both N_p and $R_{T1,T2}$ are quite well related with the maximum interstory drift, because the dispersion is small, no more than 0.12 in logarithmic terms. Also for this case, the parameter N_p results to have better relationship with the structural response; in fact, it results to be relatively more efficient with respect to $R_{T1,T2}$ for most of the scaling levels considered.

6.3. Narrow-band records

The steel frame was subjected to the set of narrow-band ground motion records. The normalized hysteretic energy obtained for the steel frame, subjected to the set of narrow-band records scaled to $Sa(T_1)=0.8$ g, is given in Fig. 14. For the case of the vectors studied, as Fig. 14 suggests, the efficiency of the vector $\langle Sa,R_{T1,T2}\rangle$ is lower with respect to $\langle Sa,N_p\rangle$. Moreover, there is a clear trend between $\langle Sa,N_p\rangle$ and the normalized hysteretic energy.

Fig. 15 demonstrates that $\langle Sa,N_p\rangle$ is more efficient than $\langle Sa,R_{T1,T2}\rangle$ for different ground motion intensity levels and in terms of maximum interstory drift and normalized hysteretic energy. Also, to clarify the potential of $\langle Sa,N_p\rangle$ for narrow-band motions, it is observed in Fig. 15a that the standard deviation of the natural logarithm for $\langle Sa,N_p\rangle$ is 0.217 while for $\langle Sa,R_{T1,T2}\rangle$ it is 0.314 for an intensity level equal to 1 g, in the case of maximum interstory drift. Moreover, the dispersion for the scalar $Sa(T_1)$ at the same intensity is equal to 0.451. The number of records required for nonlinear dynamic analysis can be explained as if the principal parameter for seismic design is the maximum interstory drift, the number of records required for nonlinear analysis to obtain the same standard error using the vector value ground motion intensity measure $\langle Sa,N_p\rangle$ is 48% of those required for $\langle Sa,R_{T1,T2}\rangle$; furthermore, the number of records for the vector here proposed is only 23% compared to the records necessary in the case of the spectral acceleration alone for a target standard error. The same conclusion is valid for normalized dissipated hysteretic energy (Fig. 15b), where the number of records required for dynamic analysis is only 28% of the records necessary for the case of $\langle Sa,R_{T1,T2}\rangle$.

7. Scaling robustness

Assessment of the scaling robustness property for the *IM* based on the parameter N_p is obtained using a subset of 34 records taken from the set of 194 ordinary records. The principal characteristic of the subset of records is that all of them have similar values of N_p. The mean value of N_p is 0.4 for the subset, the standard deviation for the N_p values was determinedly very small ($\sigma_{Np}=0.018$). The SDOF with $T_1=0.6$ s was subjected to the subset of records scaled for similar $Sa(T_1)$ values, the records were scaled in such a way that important nonlinearity was developed in the system, in this case until the median value of the ductility demand was equal to 6. Because the records were scaled for a target intensity level $Sa(T_1)$, they have similar N_p values. It is clear that all of them were scaled for similar values of the vector $\langle Sa,N_p\rangle$. For this reason, if the trend between the scale factors used in each record compared with the unbiased seismic response results is flat, the scaling robustness property is satisfied for the vector. Fig. 16 compares the scale factors with the ductility demands. It is observed that scaling records for similar values of the *IM* result as unbiased. In fact, the slope of the regression is almost horizontal for such large difference in the scale factors.

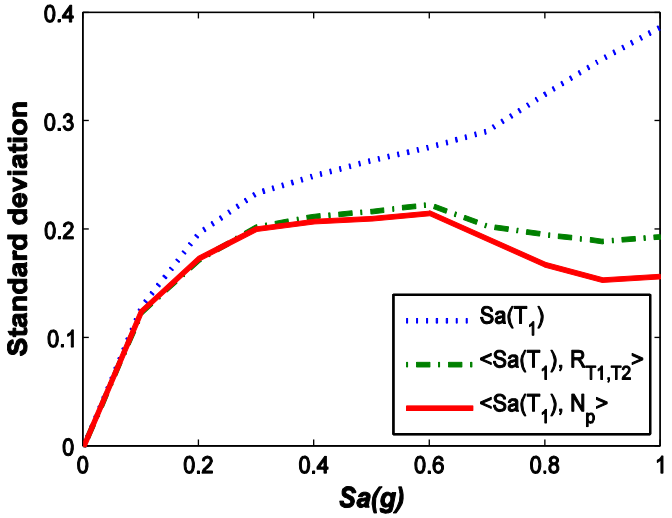

Fig. 11. Standard deviation of the natural logarithm of maximum interstory drift for $S_a(T_1)$, $\langle Sa,R_{T1,T2}\rangle$ and $\langle Sa,N_p\rangle$ at different intensity levels (R/C structure; ordinary records).

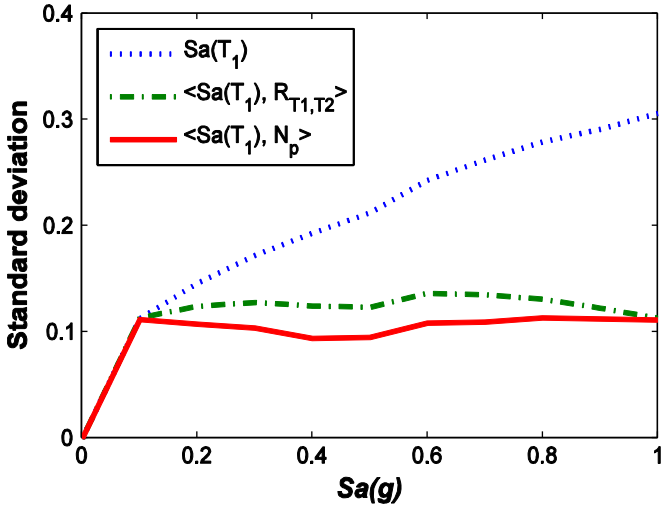

Fig. 13. Standard deviation of the natural logarithm of maximum interstory drift for $S_a(T_1)$, $\langle Sa,R_{T1,T2}\rangle$ and $\langle Sa,N_p\rangle$ at different intensity levels (R/C structure; pulse-like records).

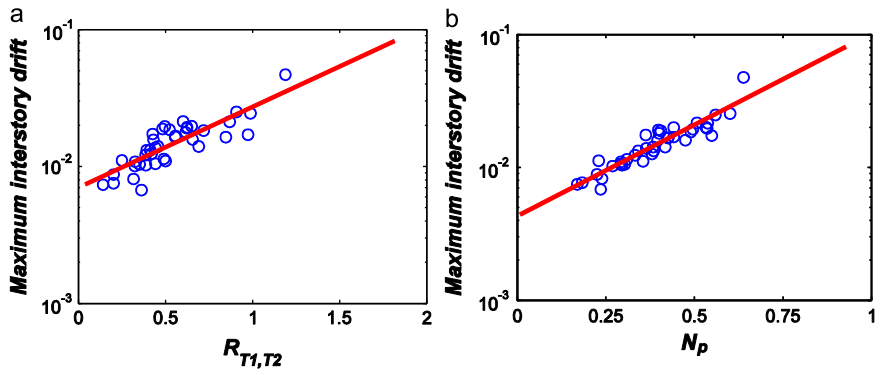

Fig. 12. Maximum interstory drift prediction for the R/C structure subjected to ordinary records ($Sa=1$ g) for (a) $R_{T1,T2}$ and (b) N_p.

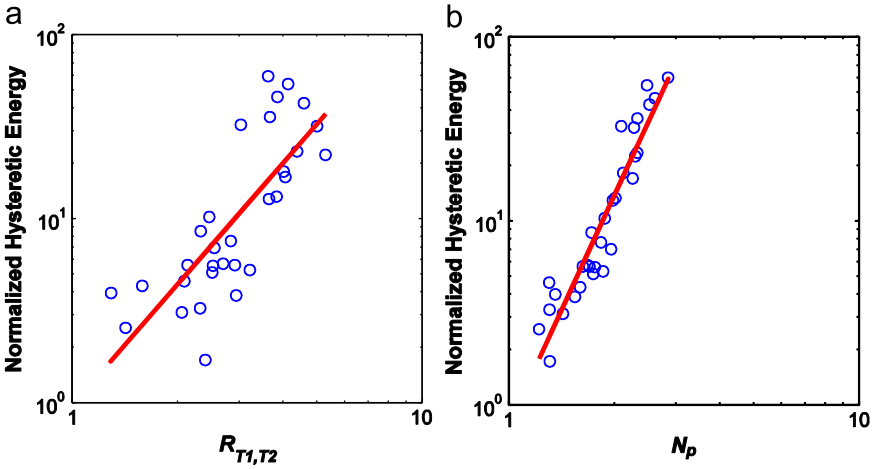

Fig. 14. Normalized dissipated hysteretic energy prediction for the moment resisting steel frame (Sa=0.8 g; narrow-band motions) for (a) $R_{T1,T2}$ and (b) N_p.

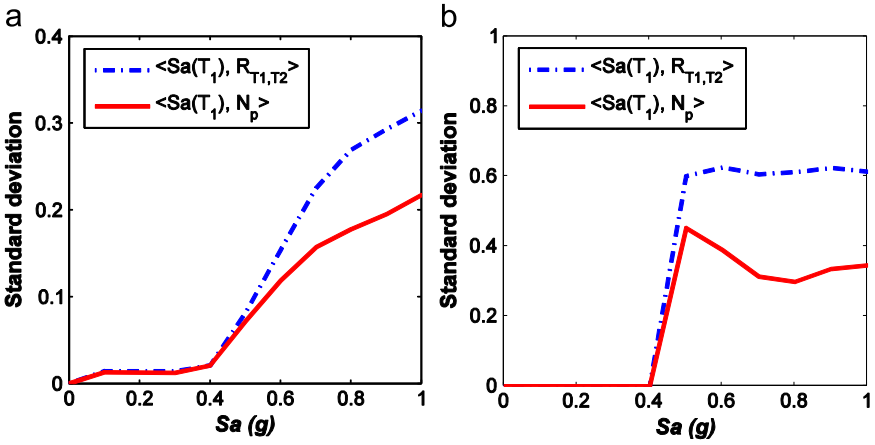

Fig. 15. Standard deviation of the natural logarithm of (a) maximum interstory drift and (b) normalized hysteretic energy for $\langle Sa,R_{T1,T2}\rangle$ and $\langle Sa,N_p\rangle$ at different intensity levels (steel frame subjected to narrow-band records).

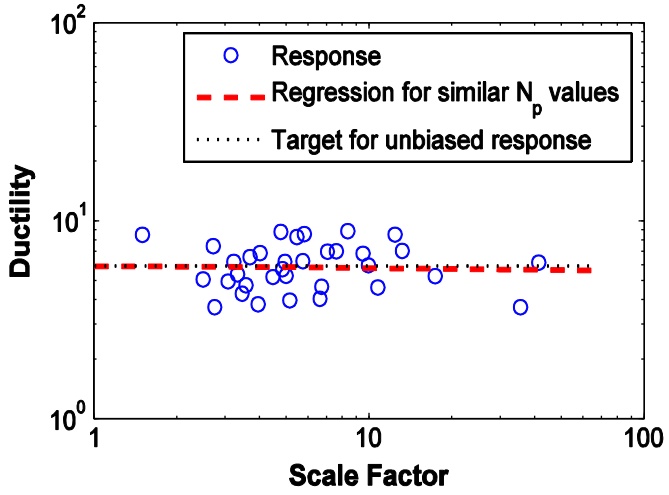

Fig. 16. Example of ductility displacement demand versus scale factor for a subset of 34 ordinary records scaled for similar values of the vector $\langle Sa,N_p\rangle$ and a SDOF (T_1=0.6 s).

8. A scalar ground motion intensity measure based on first mode spectral acceleration and N_P

Using a vector-valued intensity measure, with the aim of developing probability seismic demand analysis of a structure, requires Eq. (4), where it is necessary to evaluate two integrals and $f(N_p|Sa(T_1))$ (conditional distribution function of N_p given $Sa(T_1)$). On the other hand in the case of scalar *IMs*, the probabilistic seismic demand analysis can be carried out through Eq. (2), which is simpler. Moreover, the relationship of the *IM* with the structural response is clearer when using scalar *IMs*. Therefore, herein a scalar ground motion *IM* based on $Sa(T_1)$ and N_p with similar characteristics to the *IM* proposed by [9] is also investigated:

$$I_{Np} = Sa(T_1)\, N_p^{\alpha} \tag{8}$$

In Eq. (8) the α value has to be determined. From Eq. (8), it is possible to note that (1) the spectral acceleration at first mode of vibration is a particular case of I_{Np}, and this occurs when α is equal to zero and (2) $Sa_{avg}(T_1 \ldots T_N)$ also corresponds to the particular

Table 3
Optimal α values obtained from the analyses.

Period (s)	"Optimal α (ductility)"			"Optimal α (I_{DPA})"		
	Ordinary	Pulse-like	Narrow-band	Ordinary	Pulse-like	Narrow-band
0.5	0.4	0.4	0.4	0.4	0.5	0.5
1	0.5	0.3	0.2	0.5	0.2	0.5
1.5	0.5	0.5	0.4	0.4	0.5	0.4
2	0	0.6	0.3	0	0.6	0.3
2.5	0.4	0.6	0.5	0.4	0.6	0.4

case when $\alpha=1$. Analyses (to follow) suggest that the optimal values of α are in a range of 0–1; this means to give different weights to the contributions of the spectral accelerations beyond the first mode compared to the spectral value at T_1.

In this study, with the aim to simplify the assessment of the optimal values of α, $T_N=2T_1$ will be assumed, consistently with the results of the analyses above. α will be obtained by the analysis of nonlinear SDOF with different periods of vibration in a range from 0.5 up to 2.5 s, and it will be calibrated for maximum ductility demand, Park and Ang damage index and for a wide range of intensity levels. To limit the number of analyses, three subsets with 31 records obtained from the sets described above are used. The narrow-band set is used entirely.

Table 3 summarizes the optimal values obtained in the analysis of the structures subjected to all the record sets. The α values in all the cases are quite similar for the different record sets, the structures are analyzed and both *EDPs* are considered. For this reason, it is concluded that α is independent of the ground motion characteristic or the structure analyzed. The results in Table 3 suggest a mean value of 0.4. It is important to observe that the parameter was calibrated for the entire range of intensity levels considered.

Fig. 17 compares the steel structure subjected to the set of narrow-band motions of the maximum interstory drift for three scalar intensity measures. The first is $Sa(T_1)$, the second the scalar proposed by Cordova et al. [9] and based on $R_{T1,T2}$, and finally the scalar intensity measure proposed in this study and given by Eq. (8). To compare the similar values, the comparison of the three *IMs* was developed via incremental dynamic analysis [33] by means of the spectral acceleration, and then the specific values of the other

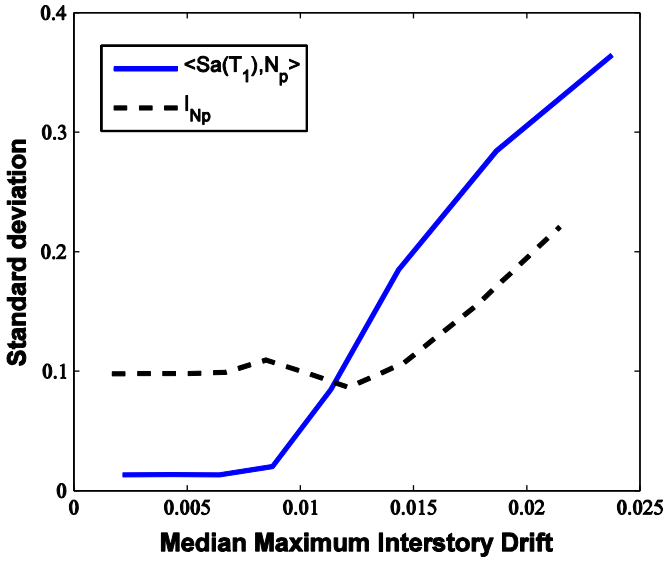

Fig. 18. $\sigma_{\langle Sa,Np\rangle|\overline{drift}}$ versus $\sigma_{I_{Np}|\overline{drift}}$ for the steel frame subjected to the set of narrow-band records at different structural demands.

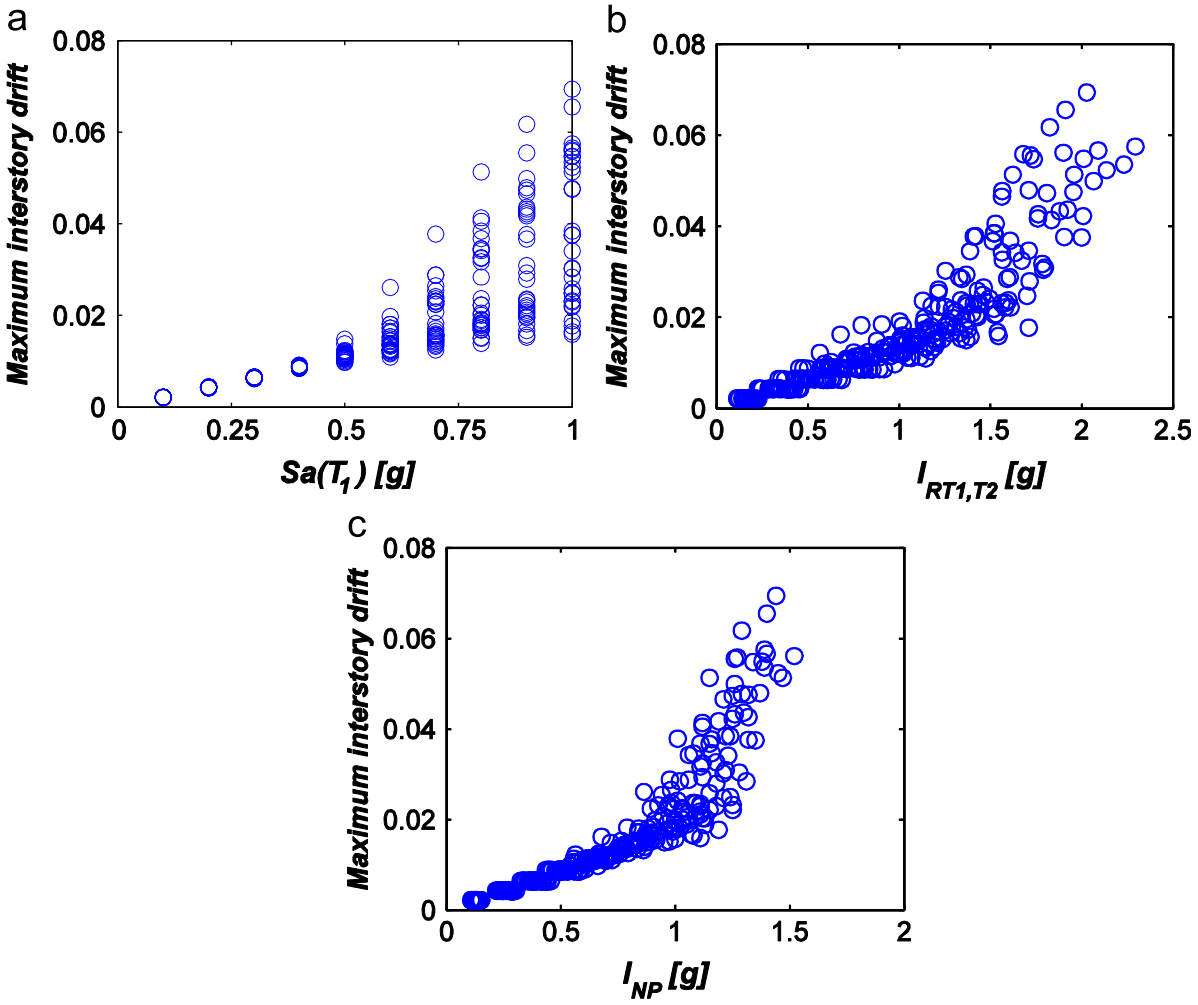

Fig. 17. Relation between scalar intensity measures and maximum interstory drift in the steel frame subjected to narrow-band motions for (a) $Sa(T_1)$, (b) $I_{RT1,T2}$ and (c) I_{Np}.

parameters associated to these results were included in the horizontal axis. The results in Fig. 17 show the potential of the ground motion intensity measure based on N_p to predict the nonlinear structural response. Moreover, there is a significant trend between I_{Np} and the maximum interstory for all the intensity levels considered.

Finally, an example of the efficiency of the scalar I_{Np} and the vector $\langle Sa,N_p \rangle$ is compared. The efficiency comparison was performed through the standard deviation of each *IM* and for a given median value of the engineering demand parameter. As example, $\sigma_{\langle Sa,Np \rangle|\overline{drift}}$ represents the standard deviation of the structural response in terms of the maximum interstory drift for the vector case, given a median maximum interstory drift ($\overline{drift}$), and $\sigma_{I_{Np}|\overline{drift}}$ is the same for I_{Np}. Fig. 18 compares the efficiency of the spectral-shape-based vector and scalar *IM* proposed here for different $\overline{drift}$ values and for the steel frame subjected to the set of narrow-band motions. For small values of $\overline{drift}$, the efficiency is larger in the case of the vector; however, the standard deviation tends to increase for the vector compared to the scalar, indicating that for large levels of the maximum interstory drift, the scalar shows relatively more efficiency.

9. Probabilistic seismic hazard analysis for I_{Np}

Because the actual possibility of computing hazard analysis is crucial for the usefulness of any proposed *IM* in this section it is shown how it can be performed for I_{Np} with ordinary tools currently available for other ground motion intensity measures. In fact, substituting Eq. (3) in Eq. (8) and applying the natural logarithm, it results in

$$\ln(I_{Np}) = \ln[Sa(T_1)] + \alpha \ln\left[\frac{Sa_{avg}(T_1 \ldots T_N)}{Sa(T_1)}\right] \tag{9}$$

Since $Sa_{avg}(T_1 \ldots T_N)$ is obtained by Eq. (10), the mean and variance of $\ln(I_{Np})$ given in Eq. (9) can be expressed as Eqs. (11) and (12).

$$Sa_{avg}(T_1 \ldots T_N) = \sqrt[N]{\prod_{i=1}^{N} Sa(T_i)} \tag{10}$$

$$E\left[\ln(I_{Np})\right] = (1-\alpha)E\left\{\ln[Sa(T_1)]\right\} + \frac{\alpha}{N}\sum_{i=1}^{N} E\{\ln[Sa(T_i)]\} \tag{11}$$

$$\begin{aligned} Var[\ln(I_{Np})] = {} & \alpha^2 Var\{\ln[Sa_{avg}(T_1 \ldots T_N)]\} + (1-\alpha)^2 Var\{\ln[Sa(T_1)]\} \\ & + 2\alpha(1-\alpha)\rho_{\ln[Sa_{avg}(T_1 \ldots T_N)],\ln[Sa(T_1)]}\sigma_{\ln[Sa_{avg}(T_1 \ldots T_N)]}\sigma_{\ln[Sa(T_1)]} \end{aligned} \tag{12}$$

The $\ln[Sa(T_i)]$ values are commonly assumed to be jointly Gaussian [34,35], and for this reason the sum also is Gaussian and $Var\{\ln[Sa_{avg}(T_1 \ldots T_N)]\}$ and $\rho_{\ln[Sa_{avg}(T_1 \ldots T_N)],\ln[Sa(T_1)]}$ can be obtained through Eqs. (13) and (14), [11]:

$$Var\left\{\ln\left[Sa_{avg}(T_1 \ldots T_N)\right]\right\} = \frac{1}{N^2}\sum_{i=1}^{N}\sum_{j=1}^{N}[\rho_{\ln[Sa(T_i)],\ln[Sa(T_j)]}\sigma_{\ln[Sa(T_i)]}\sigma_{\ln[Sa(T_j)]}] \tag{13}$$

$$\rho_{\ln[Sa_{avg}(T_1 \ldots T_N)],\ln[Sa(T_1)]} = \frac{\sum_{i=1}^{N}\rho_{\ln[Sa(T_i)],\ln[Sa(T_1)]}\sigma_{\ln[Sa(T_i)]}}{\sqrt{\sum_{i=1}^{N}\sum_{j=1}^{N}[\rho_{\ln[Sa(T_i)],\ln[Sa(T_j)]}\sigma_{\ln[Sa(T_i)]}\sigma_{\ln[Sa(T_j)]}]}} \tag{14}$$

In Eqs. (13) and (14) $\rho_{\ln[Sa(T_i)],\ln[Sa(T_j)]}$ can be evaluated for example by the relationship of Inoue and Cornell [36]:

$$\rho_{\ln[Sa(T_i)],\ln[Sa(T_j)]} = 1 - 0.33\left|\ln(1/T_i) - \ln(1/T_j)\right| \tag{15}$$

Finally, because the $\ln[Sa(T_i)]$ values are jointly Gaussian, Eqs. (11) and (12) can be obtained from actual attenuation relationship, and these equations are enough to describe the complete distribution of $\ln(I_{Np})$, and with this to perform probabilistic seismic hazard analysis as it is done for a single value of the spectral acceleration.

10. Conclusions

It has become a stronger thought in the community recently that the spectral shape is the main ground motion feature expressing the earthquake structural potential. It has been shown to be more important, for the displacement response, than source parameters or integral signal measures. This was investigated further in the study discussed in the paper comparing advanced spectral shape proxies existing and developed ad-hoc. The parameter related to spectral shape, named N_p, is intended to give direct information on the spectrum in a range of interest for the structural nonlinear shaking. Considered response parameters are related to both peak and cumulative seismic demands. Analyses include SDOF and MDOF systems comprising of concrete and steel frames.

The vectors $\langle Sa,N_p \rangle$ and $\langle Sa,R_{T1,T2} \rangle$, as expected, resulted to be better predictors compared to $Sa(T_1)$, which is used frequently for probabilistic seismic demand analysis. It was observed how the vector $\langle Sa,N_p \rangle$ shows moderately larger efficiency with respect to vectors as $\langle Sa,R_{T1,T2} \rangle$ to predict maximum displacement, hysteretic energy demands and the Park and Ang damage index in nonlinear SDOF, *R*/*C* and steel frame structures subjected to ordinary and pulse-like records.

The increased efficiency provided by $\langle Sa,N_p \rangle$ was found particularly significant for structures subjected to narrow-band motions with respect to $\langle Sa,R_{T1,T2} \rangle$. Moreover, $\langle Sa,N_p \rangle$ is less sensitive to the selection of the final period, T_N, and it is robust with respect to scaling.

For practical purposes the use of scalar *IMs* is easier than vector-valued *IMs*; a scalar *IM*, I_{Np}, was also proposed. It was found to have improved efficiency compared to the other state-of-the-art *IMs*. Finally, the study shows how probabilistic seismic hazard analysis for I_{Np} can be performed with existing tools.

It is concluded that the study of I_{Np} may give a contribution to the development of the next generation of ground motion intensity measures.

Acknowledgments

The study presented in this paper was developed within the activities of Rete dei Laboratori Universitari di Ingegneria Sismica—ReLUIS for the research program funded by the Dipartimento di Protezione Civile (2005–2008). The support given by la Secretaría de Educación Pública under F-PROMEP-38/Rev-03 SEP-23-005 and La Universidad Autónoma de Sinaloa under Grant PROFAPI 2010/018 is appreciated. The first author would like to express his gratitude to professors Gaetano Manfredi and Edoardo Cosenza for their advice during his postdoctoral studies in the Department of Structural Engineering of the University of Naples, Italy. Authors also thank Racquel K. Hagen for proofreading the paper. Finally, the very positive comments by the reviewers to this paper were very appreciated.

References

[1] Bazzurro P. Probabilistic seismic demand analysis. PhD thesis. Stanford University; 1998.
[2] Shome N. Probabilistic seismic demand analysis of nonlinear structures. PhD thesis. Stanford University; 1999.

[3] Luco N. Probabilistic seismic demand analysis, SMRF connection fractures, and near-source effects. PhD thesis. Stanford University; 2002.
[4] Iervolino I, Cornell CA. Records selection for nonlinear seismic analysis of structures. Earthquake Spectra 2005;21(3):685–713.
[5] Housner GW. Spectrum intensities of strong motion earthquakes. In: Proceedings of the symposium on earthquake and blast effects on structures. Earthquake Engineering Research Institute; 1952.
[6] Von-Thun JL, Rochin LH, Scott GA, Wilson JA. Earthquake ground motions for design and analysis of dams. In: Earthquake engineering and soil dynamics: II. Recent advance in ground-motion evaluation. Geotechnical Special Publication 20, ASCE. New York; 1988. p. 463–81.
[7] Baker JW, Cornell CA. A vector-valued ground motion intensity measure consisting of spectral acceleration and epsilon. Earthquake Engineering and Structural Dynamics 2005;34:1193–217.
[8] Tothong P, Luco N. Probabilistic seismic demand analysis using advanced ground motion intensity measures. Earthquake Engineering and Structural Dynamics 2007;36:1837–60.
[9] Cordova PP, Dierlein GG, Mehanny SSF, Cornell CA. Development of a two parameter seismic intensity measure and probabilistic assessment procedure. In: Proceedings of the second U.S.–Japan workshop on performance-based earthquake engineering methodology for reinforce concrete building structures. Sapporo, Hokkaido; 2001. p. 187–206.
[10] Baker JW, Cornell CA. Vector-valued intensity measures for pulse-like near-fault ground motions. Engineering Structures 2008;30(4):1048–57.
[11] Baker JW, Cornell CA. Spectral shape, epsilon and record selection. Earthquake Engineering and Structural Dynamics 2006;35:1077–95.
[12] Fajfar P, Krawinkler H. Conclusions and recommendations. Seismic design methodologies for the next generation of codes. A.A. Balkema; 1997.
[13] Manfredi G. Evaluation of seismic energy demand. Earthquake Engineering and Structural Dynamics 2001;30:485–99.
[14] Terán-Gilmore A, Jirsa JO. Energy demands for seismic design against low cycle fatigue. Earthquake Engineering and Structural Dynamics 2007;36:383–404.
[15] Bojórquez E, Ruiz SE, Terán-Gilmore A. Reliability-based evaluation of steel structures using energy concepts. Engineering Structures 2008;30(6):1745–59.
[16] Bojórquez E, Terán-Gilmore A, Ruiz SE, Reyes A. Evaluation of structural reliability of steel frames considering cumulative damage. In: Proceedings of the 14th world conference on earthquake engineering. Beijing, China; 2008.
[17] Bojórquez E, Terán-Gilmore A, Ruiz SE, Reyes A. Evaluation of structural reliability of steel frames: interstory drifts versus plastic hysteretic energy, Earthquake Spectra, accepted for publication.
[18] Tothong P. Probabilistic seismic demand analysis using advanced ground motion intensity measures, attenuation relationships, and near source effects. PhD thesis. Stanford University; 2007.
[19] Baker JW. Quantitative classification of near-fault ground motions using wavelet analysis. Bulletin of the Seismological Society of America 2007;97(5):1486–501.
[20] Iervolino I, Cornell CA. Prediction of the occurrence of velocity pulses in near-source ground motions. Bulletin of the Seismological Society of America 2008;98(5):2262–77.
[21] Saiidi M, Sozen M. Simple and complex models for nonlinear seismic response of reinforced concrete structures. Report UILU-ENG-79-2031. Department of Civil Engineering, University of Illinois, Urbana, Illinois; August 1979.
[22] Bojórquez E, Díaz M, Ruiz SE, García-Jarque F. Confiabilidad sísmica de varios edificios (cuatro a diez niveles) localizados en suelo blando de la Ciudad de México, diseñados con el RCDF-2004. Revista de Ingeniería Sísmica Mexicana 2007;76:1–27. In Spanish.
[23] Iervolino I, Manfredi G, Cosenza E. Ground motion duration effects on nonlinear seismic response. Earthquake Engineering and Structural Dynamics 2006;35:21–38.
[24] Park YJ, Ang AH. Mechanistic seismic damage model for reinforced concrete. Journal of Structural Engineering ASCE 1985;111(ST4):740–57.
[25] Cosenza E, Manfredi G, Ramasco R. The use of damage functionals in earthquake engineering: a comparison between different methods. Earthquake Engineering and Structural Dynamics 1993;22:855–68.
[26] Baker JW, Cornell CA. Vector-valued intensity measures incorporating spectral shape for prediction of structural response. Journal of Earthquake Engineering 2008;12(4):534–54.
[27] Baker JW. Vector-valued ground motion intensity measures for probabilistic seismic demand analysis. PhD thesis. Stanford University; 2005.
[28] Bojórquez E, Iervolino I, Manfredi G. Evaluating a new proxy for spectral shape to be used as an intensity measure. In: Proceedings of the 2008 seismic engineering conference commemorating the 1908 Messina and Reggio Calabria earthquake (MERCEA '08).
[29] Benjamin JR, Cornell CA. Probability, statistic, and decision for civil engineers. New York: McGraw-Hill; 1970.
[30] Alavi B, Krawinkler H. Effects of near-field ground motion on frame structures. Report no. 138, John A. Blume Earthquake Engineering Center, Department of Civil and Environmental Engineering, Stanford University, Stanford, CA; 2001. 301 p. http://blume.stanford.edu/Blume/TRList.htm (accessed 5/31/2006).
[31] Mavroeidis GP, Dong G, Papageorgiou AS. Near-fault ground motions, and the response of elastic and inelastic single-degree-of-freedom (SDOF) systems. Earthquake Engineering and Structural Dynamics 2004;33(9):1023–49.
[32] Fu Q. Modeling and prediction of fault-normal near-field ground motions and structural response. PhD Dissertation, Department of Civil and Environmental Engineering, Stanford University, Stanford, CA; 2005.
[33] Vamvatsikos D, Cornell CA. Incremental dynamic analysis. Earthquake Engineering and Structural Dynamics 2002;31:491–514.
[34] Bazzurro P, Cornell CA. Vector-valued probabilistic seismic hazard analysis. In: Proceedings of the 7th US national conference on earthquake engineering. Earthquake Engineering Research Institute, Boston, MA; 2002.
[35] Stewart JP, Chiou SJ, Bray JD, Graves RW, Somerville PG, Abrahamson NA. Ground motion evaluation procedures for performance-based design. Soil Dynamics and Earthquake Engineering 2002;22:765–72.
[36] Inoue T, Cornell CA. Seismic hazard analysis of multi-degree-of-freedom structures. reliability of marine structures, RMS-8. Stanford, CA; 1990.